Full polarization analysis of resonant superlattice and forbidden x-ray reflections in magnetite

2009 J. Phys.: Condens. Matter 21 485601

(http://iopscience.iop.org/0953-8984/21/48/485601)

J. Phys.: Condens. Matter **21** (2009) 485601 (9pp) doi:10.1088/0953-8984/21/48/485601

Full polarization analysis of resonant superlattice and forbidden x-ray reflections in magnetite

S R Bland[1], B Detlefs[2], S B Wilkins[3], T A W Beale[1], C Mazzoli[2], Y Joly[4], P D Hatton[1], J E Lorenzo[4] and V A M Brabers[5]

[1] Department of Physics, University of Durham, Durham DH1 3LE, UK
[2] European Synchrotron Radiation Facility, 6 rue Jules Horowitz, BP 220, F-38043 Grenoble, France
[3] Condensed Matter Physics and Materials Science Department, Brookhaven National Laboratory, Upton, NY 11973-5000, USA
[4] Institut Néel, CNRS and Université Joseph Fourier, BP 166, F-38042, Grenoble, Cedex 9, France
[5] Department of Physics, Eindhoven University of Technology, NL-5600, MB Eindhoven, The Netherlands

E-mail: p.d.hatton@durham.ac.uk

Received 25 August 2009, in final form 13 October 2009
Published 30 October 2009
Online at stacks.iop.org/JPhysCM/21/485601

Abstract

Despite being one of the oldest known magnetic materials, and the *classic* mixed valence compound, thought to be charge ordered, the structure of magnetite below the Verwey transition is complex and the presence and role of charge order is still being debated. Here, we present resonant x-ray diffraction data at the iron K-edge on forbidden $(0,\ 0,\ 2n+1)_C$ and superlattice $(0,\ 0,\ \frac{2n+1}{2})_C$ reflections. Full linear polarization analysis of the incident and scattered light was conducted in order to explore the origins of the reflections. Through simulation of the resonant spectra we have confirmed that a degree of charge ordering takes place, while the anisotropic tensor of susceptibility scattering is responsible for the superlattice reflections below the Verwey transition. We also report the surprising result of the conversion of a significant proportion of the scattered light from linear to nonlinear polarization.

(Some figures in this article are in colour only in the electronic version)

1. Introduction

Magnetite has long been a subject of interest, with curiosity dating back to the discovery of lodestone and its magnetic properties [1]. More recently, magnetite has been regarded as a model compound in several respects; magnetite is the first material in which a low temperature charge ordered (CO) structure was proposed, as well as being a classic ferrimagnetic system. At room temperature magnetite has an inverse cubic spinel structure, with space group $Fd\bar{3}m$ (no. 227) and $a_C = 8.394$ Å. The chemical formula is often written as $Fe^{3+}[Fe^{2+}Fe^{3+}]O_4$ to highlight the mixed valence nature. Here, the first term corresponds to Fe^{3+} ions in tetrahedrally coordinated (A) sites and the second term to Fe^{2+} and Fe^{3+} ions in octahedrally coordinated (B) sites. The B sites are occupied by divalent and trivalent Fe ions which possess no long range charge order; however, in order to explain the large, spontaneous increase in resistivity upon cooling below $\approx$120 K (T_V), Verwey [2] proposed an ordering of the B-sited iron atoms with Fe^{3+} and Fe^{2+} layers stacking along the $[0\ 0\ 1]_C$ direction, separated by a quarter unit cell. This original description agrees with Anderson's criteria [3] for charge ordering, whereby the Coulomb energy of the system is reduced. However, it has become clear that this purely ionic picture may be incorrect, and debate continues as to whether the low temperature ground state can be described using a simplistic Fe^{2+} and Fe^{3+} ionic model. Total ionic separation has been demonstrated to be incorrect from the Kerr effect [4] and diffraction [5] measurements, and further supported on

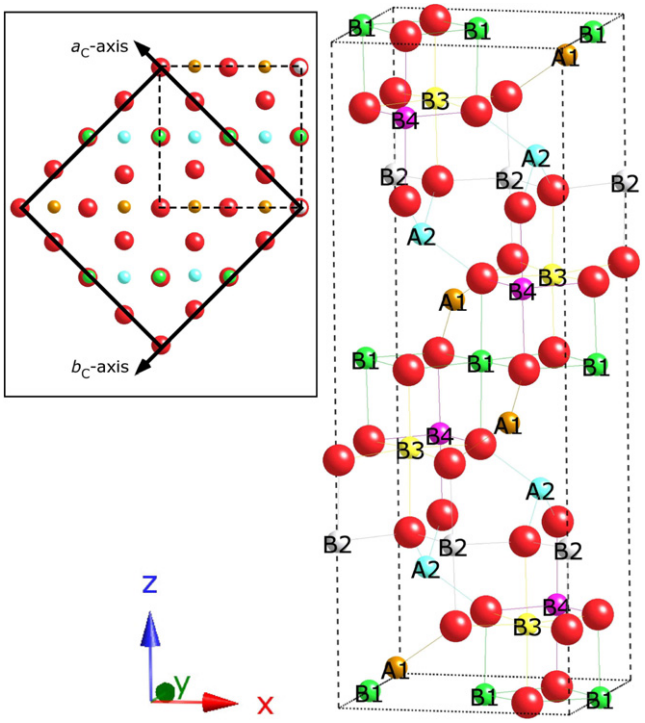

Figure 1. The simplified low temperature structure of magnetite, in the orthorhombic *Pmca* refined unit cell. Fe^{3+} ions sit at tetrahedral A sites while charge ordering takes place over the four inequivalent octahedral B sites. Oxygens sit at the corners of the polyhedra. In the $P2/c$ cell there are six inequivalent B sites. The inset shows the view along the *c* axis, showing the high temperature cubic cell as a solid black line and the orthorhombic cell as a dashed line.

entropic [6] and theoretical grounds [7]. A recent resonant x-ray scattering (RXS) experiment has also suggested that the phase transition may actually be continuous, with electronic order appearing approximately 10 K above T_V [8].

Below T_V the symmetry of the crystal structure is significantly lowered and is believed to adopt a *Cc* structure (no. 9): recent RXS results have been used to provide the first refinement in the *Cc* unit cell [9]. The low temperature structure is remarkably complex even in the simpler $P2/c$ (no. 13) refinement [10, 11]. This structure, refined using *Pmca* (no. 57) constraints, contains six inequivalent B sites, making the determination of the charge ordered structure rather complicated. The simpler, orthorhombic *Pmca* refined structure, with lattice parameters $a_O = 5.944$ Å, $b_O = 5.924$ Å and $c_O = 16.775$ Å is shown in figure 1. Theoretical studies [4] have suggested that charge ordering occurs along the $[0\,0\,1]_C$ direction with a modulation wavevector of $(0\,0\,1)_C$ and an additional minor modulation of $(0\,0\,\frac{1}{2})_C$, where the *C* denotes indexing using the high temperature cubic unit cell. Theoretical studies have also proposed that orbital ordering may occur on the electron-rich Fe^{2+} B sites [7, 12, 6, 13].

Resonant x-ray scattering is the ideal tool for attempting to resolve questions of the presence and magnitude of long range correlation effects in ordered materials. Recent RXS studies [14–16] of the forbidden $(0\ 0\ 2)_C$ and $(0\ 0\ 6)_C$ reflections have reported that they are present *above* the Verwey transition and do not change upon passing through T_V.

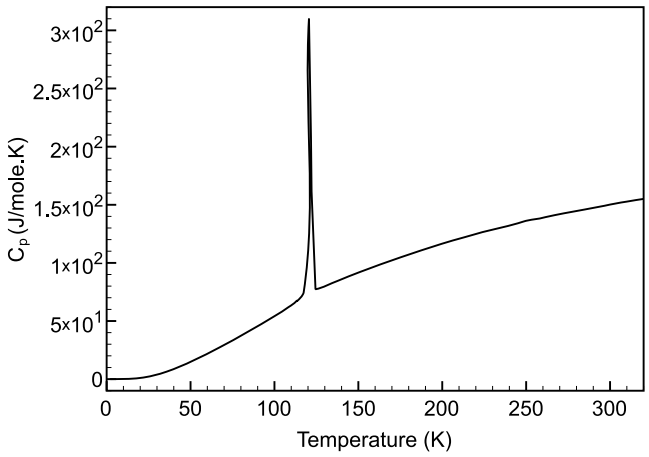

Figure 2. The heat capacity of magnetite, clearly showing the phase transition at T_V.

In these studies it was shown that the forbidden reflections were not an effect of charge order and that local anisotropy at the iron octahedral sites alone was enough to explain the forbidden $(0,\ 0,\ 4n+2)_C$ reflections. Further attempts to use RXS to identify $(0,\ 0,\ \frac{2n+1}{2})_C$ and strong $(0,\ 0,\ 2n+1)_C$ reflections at the iron K-edge have proven difficult and studies using a variety of other reflections such as $(h\ k\ \frac{2n+1}{2})_C$ and $(\bar{k}\ k\ l)_C$ in order to determine the presence of charge order have suggested that the charge disproportionation is either small or non-existent [17, 5]. In order to address this issue, we have performed an RXS experiment on a high quality, single crystal of magnetite, subjecting the sample to full polarization analysis of the diffracted signal.

2. Experiment

Specific heat measurements, figure 2, were performed on the crystal to confirm the purity, which is difficult to grow with the correct oxygen stoichiometry. A small specimen of magnetite was obtained from the same growth boule as used for the scattering experiment. The sample was a synthetically grown crystal of Fe_3O_4, grown using the floating zone method in an image furnace [18]. The measurements, performed on a Quantum Design PPMS, revealed the Verwey transition to be at 120.4 ± 0.3 K with the transition peak possessing a full width at half-maximum of ≈ 3 K and an entropy of transition, ΔS_V, of 5.8 ± 0.3 J mol^{-1} K^{-1}. This is a lower temperature than the value reported by Kim-Ngan *et al* [19] of 123.5 K for a stoichiometrically correct sample, which displayed a heat capacity peak width of 0.2 K and ΔS_V of 6.4 J mol^{-1} K^{-1}. However, despite the differences in transition temperatures and ΔS_V it is clear that the sample was well within the first-order transition region [20, 21] (given by $\delta < 0.0012$, where $Fe_{3(1-\delta)}O_4$) and with purity above $\delta \leqslant 0.0007$.

The x-ray diffraction experiment was performed at the iron K-edge on ID20 at the European Synchrotron Radiation Facility, Grenoble, France. The experiment was carried out using the four-circle diffractometer in vertical scattering geometry, with a diamond phase plate placed in the x-ray beam to allow the rotation of the incident linear polarization through

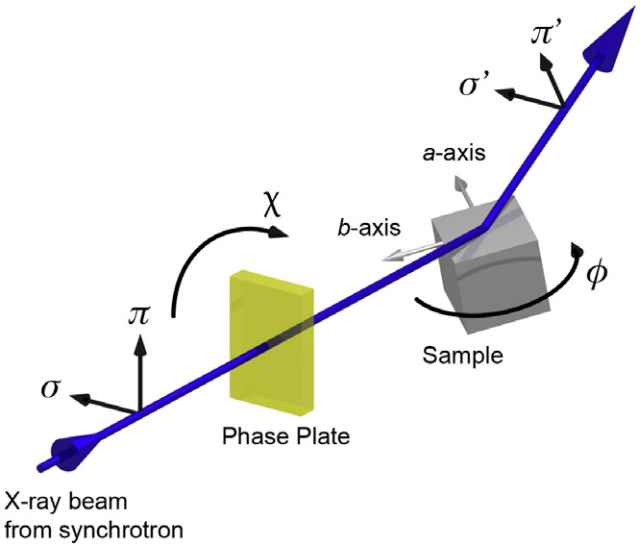

Figure 3. Experimental layout highlighting the crystal orientation and sense of the polarization rotation. The phase plate acts as a half-wave plate, allowing the polarization of the x-rays to be rotated away from the initial horizontal (σ) polarization, to any arbitrary linear polarization, by rotating the phase plate itself, χ. Here ϕ represents the angle between the a_C axis and the scattering plane, with respect to the direction of the beam.

180° from the normally incident σ-polarized radiation. The basic experimental layout showing the direction of rotation is outlined in figure 3. The technique of rotating the incident polarization has been demonstrated previously to allow the determination of otherwise unresolvable mixed multipolar contributions to the scattering [22], the relative contributions of magnetic domains [23] and the determination of magnetic moment directions [24]. The intensity of the outgoing linear polarization was measured by subsequently scattering from an MgO (2 2 2) analyser crystal. A small $\sim$ 0.3 T magnet, approximately the same size as the sample, was attached to the top of the copper sample mount using silver paint and the magnetite crystal mounted on top of the magnet using another layer of silver paint. The field was applied along one of the $\langle 0\ 0\ 1\rangle_C$ axes to fix and uniquely define the monoclinic c axis on cooling through T_V [25].

3. Polarization dependence and anisotropic tensor of susceptibility reflections

The procedure of rotating the polarization of incident linear light is similar to the more familiar practice of performing an azimuthal rotation of the sample; however, by rotating the plane of incident polarization rather than the sample itself, the sample may be kept stationary in the x-ray beam and the problem of contamination from Renninger reflections [26] (multiple scattering) is eliminated. This elimination is the result of being able to selectively choose a single azimuthal orientation such that Renninger reflections at the chosen energy are excluded. Further, since the sample need not be rotated, the technique is less sensitive to contributions from different domain populations in the sample. To perform the polarization analysis, an azimuthal position clear of multiple scattering was selected and the polarization of the incident light rotated through 180° from σ to π to σ, in the direction indicated in figure 3. To extract the polarization information of the diffracted signal the analyser crystal was rotated through 180° for each value of the incident polarization. The dependence of the intensity on the angle of the analyser crystal allowed the linear components of the familiar self-normalized Stokes parameters [27] to be extracted:

$$P_1 = \frac{(I_{\sigma'} - I_{\pi'})}{I_0}, \tag{1}$$

$$P_2 = \frac{(I_{+45^{\circ}{}'} - I_{-45^{\circ}{}'})}{I_0}, \tag{2}$$

where I_0 represents the total scattered intensity. We are unable to directly measure the circularly polarized components to find P_3:

$$P_3 = \frac{(I_{\text{right circular}'} - I_{\text{left circular}'})}{I_0}. \tag{3}$$

However, an upper limit for P_3 can be deduced by subtraction:

$$P_{N-L}^2 = 1 - P_1^2 - P_2^2. \tag{4}$$

The importance of polarization becomes apparent close to the absorption edge, where the scattering factor must be expressed as a tensor series as part of the multipolar expansion. For non-magnetic contributions the total scattered amplitude may be expressed as

$$f(\epsilon, \epsilon') = \epsilon \cdot \epsilon' f^0 + \sum_{m,n} \epsilon_m \epsilon'_n \hat{S}^0_{mn} + \sum_{m,n,o} (\epsilon_m \epsilon'_n k'_o - \epsilon'_m \epsilon_n k_o) \hat{T}^0_{mno} + \cdots, \tag{5}$$

where ϵ and ϵ' represent the incident and scattered polarization, respectively, f^0 is the scalar scattering term and $\mathbf{k}$ is the wavevector. Of the tensorial terms, only the lower rank members are typically strong, and in continuing we will restrict discussion to terms no higher than the electric quadrupole (E1–E1) term. As such, only the terms f^0 and $\hat{S}^0$ need be considered. For the case of scattering from electric transitions, the tensors $\hat{S}^0$ and higher are symmetric. When the scalar scattering factor term becomes zero due to the systematic absences of compound (non-symmorphic) symmetry operations, anisotropic tensorial terms can still be allowed. Reflections observed at such positions are referred to as Templeton–Templeton [28] or ATS (anisotropy of the tensor of susceptibility) [29] type reflections. With regard to the analysis that follows we point out that it is the first scalar term in equation (5) which is responsible for Bragg and charge order reflections, while it is the second term that is responsible for anomalous charge and ATS scattering. Thus the appearance of a reflection at T_V is not necessarily an indication of charge order, but may be the result of a structural transition changing the local environment of the resonating atom.

To demonstrate the form of these tensors we use the $Pmca$ structure refined by Wright *et al* [10, 11]. The construction of these tensors is a relatively simple matter when the crystal structure with the correct space group is known, as the tensor at

each atomic position is symmetric under its own site symmetry and related to the equivalent Wyckoff positions through the appropriate symmetry operations. The final tensor, $\hat{S}^0$, is then produced by combining the individual tensors in a structure factor calculation:

$$f^0 = \sum_{\mathbf{r}_j} f_j e^{i\mathbf{q}\cdot\mathbf{r}_j}; \qquad \hat{S}^0 = \sum_{\mathbf{r}_j} \hat{S}_j e^{i\mathbf{q}\cdot\mathbf{r}_j}, \tag{6}$$

where f_j and $\hat{S}_j$ represent scalars and tensors, respectively, for atoms at positions $\mathbf{r}_j$. Using the *Pmca* structure we find that for the $(0,\ 0,\ \frac{1}{2})_C$ and $(0,\ 0,\ \frac{9}{2})_C$ reflections the only elements of the tensor that may contribute are the Q_{yz} components:

$$f^{(0,\ 0,\ \frac{1}{2})_C} = 0; \qquad \hat{S}_{\mathrm{ATS}}^{(0,\ 0,\ \frac{1}{2})_C} = \begin{pmatrix} 0 & 0 & 0 \\ 0 & 0 & Q_{yz} \\ 0 & Q_{yz} & 0 \end{pmatrix}, \tag{7}$$

with allowed contributions from all iron sites *except* B2.

For the $(0\ 0\ 1)_C$ and $(0\ 0\ 5)_C$ reflections in the *Pmca* structure we find that

$$f^{(0\ 0\ 1)_C} = f^0; \qquad \hat{S}_{\mathrm{ATS}}^{(0\ 0\ 1)_C} = \begin{pmatrix} Q_{xx} & 0 & 0 \\ 0 & Q_{yy} & 0 \\ 0 & 0 & Q_{zz} \end{pmatrix}, \tag{8}$$

with all iron sites contributing. We point out here that a signal from pure charge order is now allowed from both the scalar and tensor components.

We note here that, as the symmetry is reduced to the $P2/c$ unit cell, an additional Q_{xy} term becomes allowed for the $(0,\ 0,\ \frac{1}{2})_C$ and $(0,\ 0,\ \frac{9}{2})_C$ reflections. However, this term is expected to be negligible, as it is related to the small monoclinic distortion and so is effectively attenuated by a factor of $\sim|\cos(\beta)| = 0.004\,11$. As pointed out by others [30, 31], the diagonal terms in equations (7) go to zero and so this reflection cannot represent a charge order signal. Further, the presence of this reflection is also not necessarily a direct consequence of orbital order, as has previously been made clear [31, 32]. In magnetite alone ATS reflections have previously been confirmed as being responsible for the forbidden $(0\ 0\ 2)_C$ and $(0\ 0\ 6)_C$ reflections above [33, 14, 15] and below [16] T_V.

As mentioned above, the development of ATS reflections in the close neighbourhood of an absorption edge is related to the presence of compound symmetry elements (screw axis, glide planes or both simultaneously) in the space group. Reflections which are not forbidden by these non-symmorphic *or* symmorphic symmetry operations result in any anisotropy of the local environment being hardly visible from the point of view of resonant x-ray diffraction, as the reflections contain information on the isotropic part of the tensor that is often much larger than the anisotropic part. An exception to this *rule* is certainly the $(0,\ 0,\ 4n+2)$ reflections below T_V, where the isotropic part nearly cancels out, but not completely.

In magnetite the $(0,\ 0,\ 4n+2)$ reflections originate from the small trigonal distortion that the octahedrally sited irons experience as a result of the nearest-neighbour atomic environment. From the electronic point of view each octahedral site has a single occupancy of all the orbitals in a high spin configuration, $3(t_{2g}^{\uparrow})2(e_g^{\uparrow})$, with an extra (half) electron of opposite spin giving rise to the half metallic properties. In a band theory picture, the former electrons are in bands below the Fermi energy level (E_F) whereas the latter are in a band above E_F. This trigonal distortion has the important effect of lifting the degeneracy of the t_{2g} orbitals (triplet) into a singlet (a_{1g}) and a doublet (e_g). The former is the lowest lying level and might be considered as the ground state. It is interesting to remark that resonant x-ray experiments at the iron K-edge reveal the symmetry of the local distortion at the octahedral sites which in turn affects the symmetry of the crystal field levels. This relationship between local distortions and the breaking of the electronic symmetry means that it is indeed possible to learn about the orbital ordering. In the case of the cubic phase of magnetite, the direction of the local anisotropy is the [1 1 1] yielding a complex geometrical arrangement of the a_{1g} and e_g orbitals throughout the lattice.

In magnetite below T_V one may think that there can be no orbital ordering as the ground state is a singlet. No further energy gain can be achieved in magnetite according to this picture. However, as pointed out in the early studies on magnetite, the gap between the singlet and the doublet, of 150 meV, is much smaller than the bandwidth of the corresponding band. Therefore one should consider the complete basis a_{1g} and e_g with different possibilities for occupation by the extra electron with opposite spin and an incipient possibility for orbital ordering and energy gain due to possible splitting of the e_g orbitals. The phase diagram of possible ground states below T_V as a function of the inter-site repulsion and the electron hopping has been recently worked out by Uzu and Tanaka [34, 13]. Band structure calculations have pointed out that orbital ordering occurs in the low temperature phase of magnetite. This should be evident as the extra electron, $e^{\downarrow}$, ought to choose between one of the three t_{2g} orbitals.

In general, the occurrence of ATS reflections as a result of a phase transition, in addition to signalling the manifestation of a non-symmorphic space group, implies that some local symmetry has been broken. If this symmetry breaking raises some orbital degeneracy in the ground state then we will have a situation that we could classify as giving rise to orbital ordering. However, the ATS is not a pure manifestation of orbital ordering, and it may well be that the orbital ordering component is not the strongest contribution to the local anisotropy, although, in any case, the ATS reflections should, in some manner, convey information about this orbital ordering.

4. Results and discussion

After cooling below the Verwey transition and tuning the photon energy to the iron K-edge, scans along the L direction in reciprocal space were conducted, figure 4, which clearly identify a number of half and odd integer reflections. The widths of the reflections, figure 5, measured in this study are an order of magnitude smaller than in the previous study by Lorenzo *et al* [8], particularly for the $(0,\ 0,\ \frac{9}{2})_C$ reflection. At 20 K we determine inverse correlation lengths

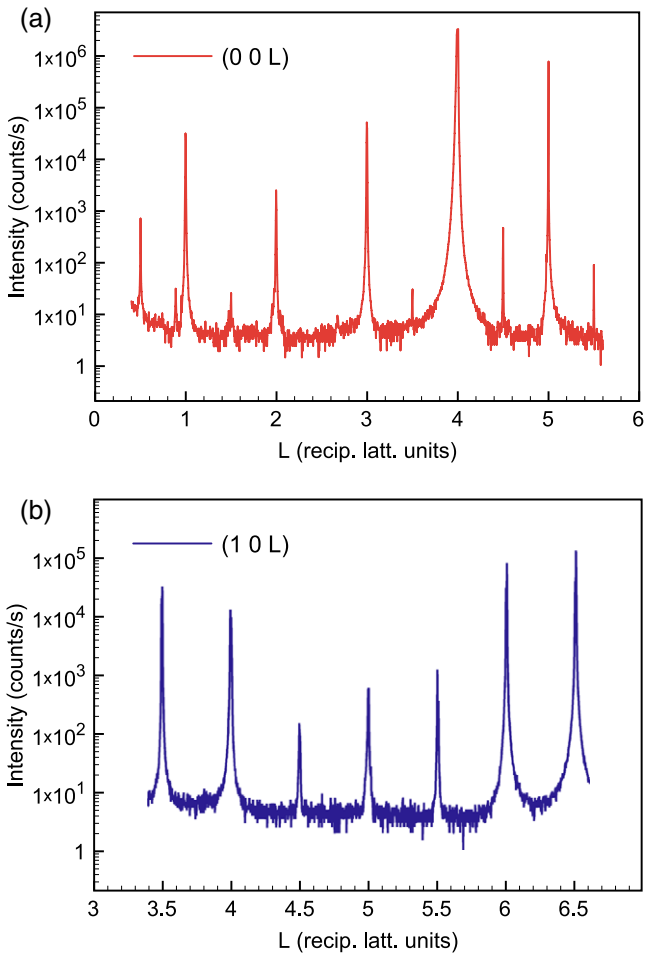

Figure 4. Scans along (a) the L axis and (b) $[1\ 0\ L]_C$ axis in reciprocal space at 20 K, tuned to 7.120 keV in the σ–σ channel. The detector saturated whilst moving through the $(0\ 0\ 4)_C$ reflection, although supplementary scans indicate the corresponding intensity was approximately 400×10^6 counts s^{-1}. A weak $(0\ 0\ \frac{5}{2})_C$ reflection was also located on separate scans.

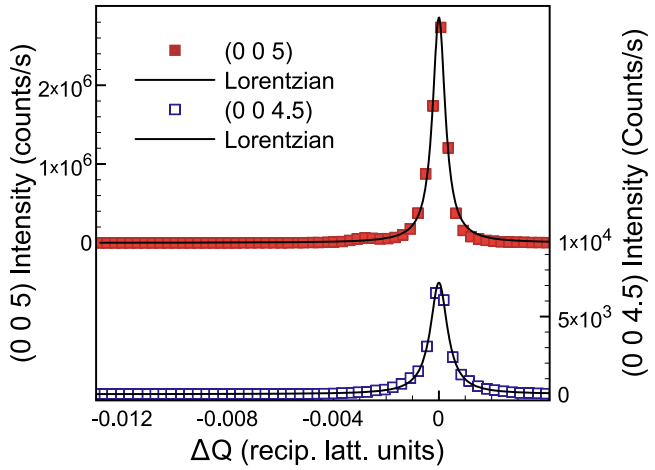

Figure 5. Scans along the L axis of the $(0,\ 0,\ \frac{9}{2})_C$ and $(0\ 0\ 5)_C$ reflections, tuned to 7.12 keV at 20 K in the σ–σ channel. The peaks have been artificially shifted to the origin for ease of comparison. Both reflections show a similar width, although the $(0,\ 0,\ \frac{9}{2})_C$ reflection is significantly weaker in this channel.

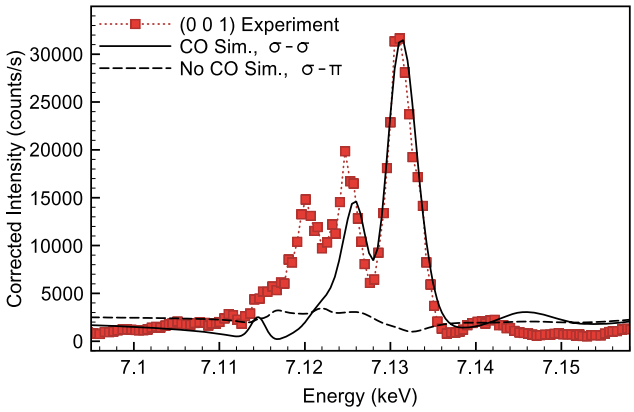

Figure 6. The energy dependence of the $(0\ 0\ 1)_C$ reflection at 20 K in the σ–σ channel, measured at fixed wavevector. The experimental dependence has been corrected for multiple scattering and absorption effects. The solid (dashed) line represents a simulation with (without) charge order. The simulation axes have been scaled for the optimum fit and the corrected intensity represents an order of magnitude estimate based on figure 4(a).

of 2.94×10^{-4} and 2.18×10^{-4} Å^{-1} for the $(0,\ 0,\ \frac{9}{2})_C$ and $(0\ 0\ 5)_C$, respectively. The $(0\ 0\ 5)_C$ peak was later shown to be approximately one-third broader than the $(0\ 0\ 4)_C$ Bragg reflection, indicating that the orders responsible for the additional reflections below the Verwey transition were indeed well correlated. The presence of the $(0,\ 0,\ \frac{n}{2})_C$ reflections at the iron K-edge is in contrast to the previous study by Subias *et al* [17] who also used RXS to attempt to observe these peaks. The improved signal-to-noise ratio in our study, of greater than three orders of magnitude over the previous study, is most likely the reason we were able to detect the half-integer reflections. Further, the initial scan along the L axis conducted in the earlier study, corresponding to figure 4(a), was performed over the region containing the weaker superlattice reflections between $\sim(0\ 0\ 2)_C$ and $\sim(0\ 0\ 4)_C$. In that study it was concluded that the lack of resonant enhancement of the $(0,\ 0,\ 2n+1)_C$ reflections, along with the complete lack of $(0,\ 0,\ \frac{2n+1}{2})_C$ reflections, indicated that any charge segregation must be non-integer; with a maximum disproportionation of $0.1e^-$. However, soft resonant x-ray diffraction experiments have also previously seen the $(0,\ 0,\ \frac{1}{2})_C$ reflection at the oxygen K-edge and iron L_2-edge [35, 30, 31], as has another recent study at the iron K-edge [8].

Reflections which can be indexed as $(0,\ 0,\ 2n+1)_C$ and $(0,\ 0,\ \frac{2n+1}{2})_C$ were found to resonate; however, due to the high quality of the crystal sample, and the large size of the crystallographic unit cell below T_V, the experiment was particularly sensitive to the problem of Renninger reflections. The resonances depicted in figures 6–9 were thus identified by performing multiple energy scans at slightly offset azimuthal positions, allowing the separation of the superlattice and Renninger reflections through the production of a composite scan. To obtain an accurate fit to the degree of charge segregation, a much greater number of reflections

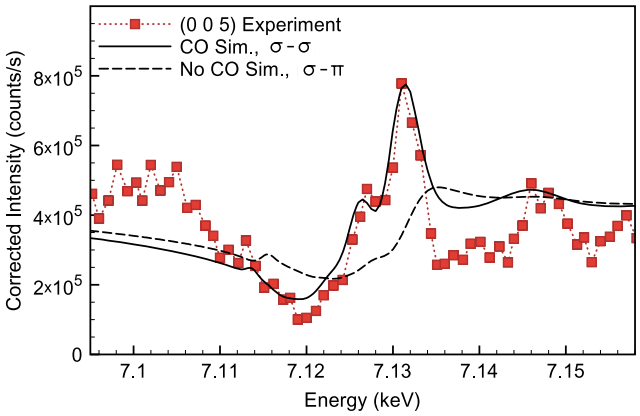

Figure 7. The energy dependence of the $(0\ 0\ 5)_C$ reflection at 20 K in the σ–σ channel, measured at fixed wavevector. The experimental dependence has been corrected for multiple scattering and absorption effects. The solid (dashed) line represents a simulation with (without) charge order. The simulation axes have been scaled for the optimum fit and the corrected intensity represents an order-of-magnitude estimate based on figure 4(a).

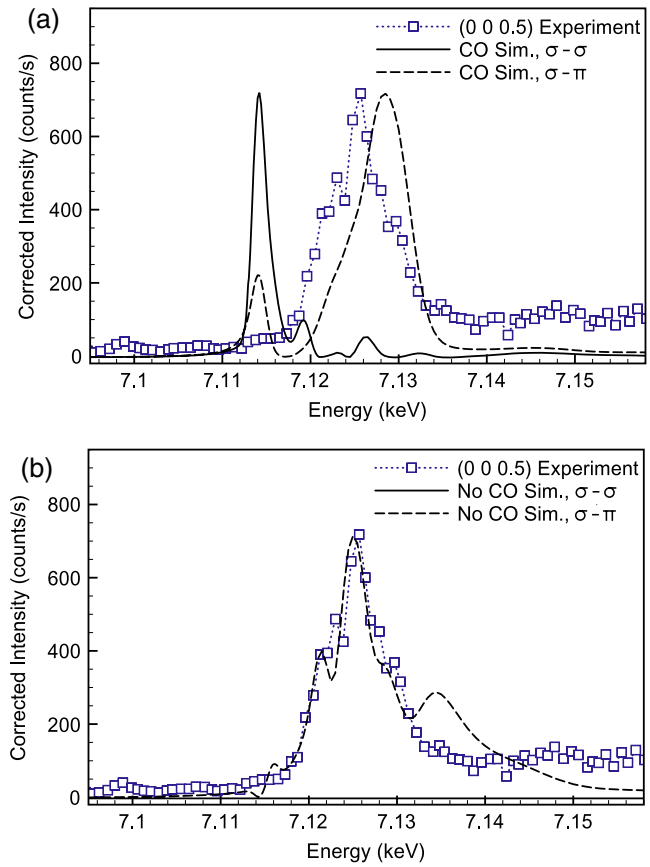

Figure 8. The energy dependence of the $(0,\ 0,\ \frac{1}{2})_C$ reflection at 20 K in the σ–σ channel, measured at fixed wavevector. The experimental dependence has been corrected for multiple scattering and absorption effects. The solid and dashed lines represent simulations with charge order (a) and without charge order (b). Although the dependence was measured in the σ–σ channel, the leakthrough from the σ–π channel was measured to be ∼0.92% and show the σ–π simulation is shown with an attenuation of ∼99.08% relative to the σ–σ simulation. The simulation axes have been rescaled for the optimum fit and the corrected intensity represents an order of magnitude estimate based on figure 4(a).

is required, as used in Nazarenko *et al*, and so in this case a simplified charge order model based on the most recent refined structure is used. The models with and without charge ordering in figures 6–9 were produced using the FDMNES programme [36] using the Cc structure derived from the $Pmca$ structure of Wright *et al* [11], using a charge disproportionation of $0.1e^-$ between the B1 and B2 sites only [9]. The simulation does not include the magnetic structure, which is expected to have negligible effect. The simulations used the Hedin and Lundqvist exchange correlation potential [37], a 7 Å cluster radius, and were run using full multiple scattering theory rather than the finite difference method.

It is clear from figures 6 and 7 that there is a much stronger agreement with the data for the $(0\ 0\ 1)_C$ and $(0\ 0\ 5)_C$ reflections when charge order is considered than without, with the full spectra corresponding to E1–E1 processes from both octahedral and tetrahedral sites, despite charge order itself only present on the octahedral sites (B1 and B2). For the $(0,\ 0,\ \frac{2n+1}{2})_C$ type reflections in figures 8 and 9, it is difficult to draw any conclusions regarding the presence (or lack of) charge order, at first glance. Figure 8 appears to show a closer agreement without charge order, whereas figure 9 arguably shows a better agreement with charge order. One argument against the charge order simulation of figure 9 is that there does not appear to be any indication of the large pre-edge feature, present in both channels: the combined effect is thus the feature we would expect to be dominant. From studying the results of the calculation we see that the pre-edge features, in the simulations for both $(0,\ 0,\ \frac{2n+1}{2})_C$ type reflections, primarily originate from the tetrahedral sites, while the feature which is higher in energy (corresponding to the measured signal) originates *almost* entirely from the octahedral sites. We note here that the spectra of the $(0,\ 0,\ \frac{2n+1}{2})_C$ type reflections are highly sensitive to the crystallographic structure, and so it is not particularly surprising that the simulation does not fully replicate the experimental data.

To perform further analysis on both $(0,\ 0,\ \frac{2n+1}{2})_C$ and $(0,\ 0,\ 2n+1)_C$ type reflections, and confirm their origins, we selected the $(0,\ 0,\ \frac{9}{2})_C$ and $(0\ 0\ 5)_C$ peaks. These reflections demonstrated Lorentzian lineshapes, figure 5, and upon warming were found to remain relatively stable in position and correlation length, up to T_V, where the signal promptly disappeared: typical behaviour of a first-order phase transition. This behaviour of the $(0,\ 0,\ \frac{9}{2})_C$ reflection is in contrast to the $(0,\ 0,\ \frac{1}{2})_C$ temperature dependence that was recently measured using RXS [8], which displayed no significant drop in intensity at T_V. However, the validity of these results has been questioned [32]. We are continuing to investigate the origins of these differences, which we suspect to be sample-dependent. The iron K-edge results presented here are consistent with recent soft x-ray studies at the iron L_3 and oxygen K-edges [31] which used very high quality single crystals from the same source and find a similar first-order extinction of the $(0,\ 0,\ \frac{1}{2})_C$ reflection at T_V.

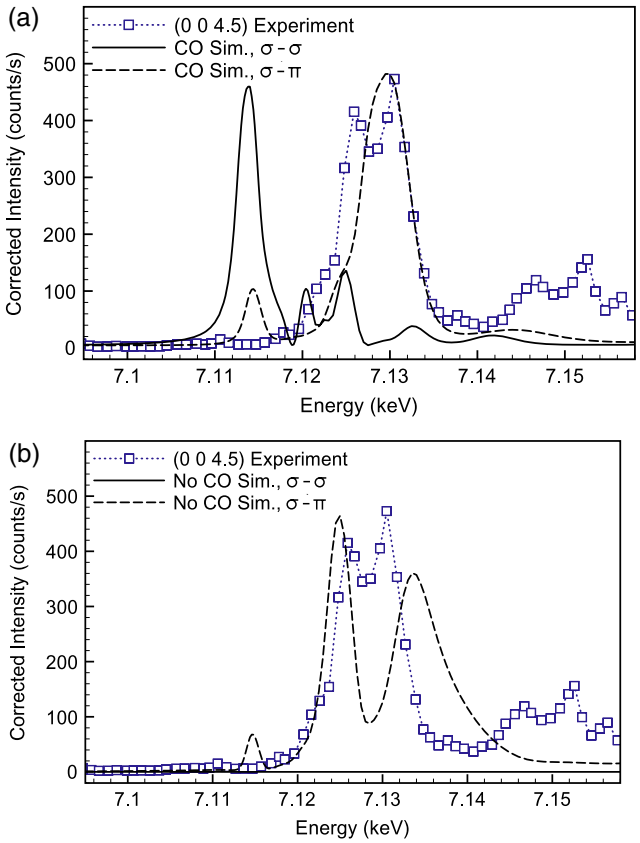

Figure 9. The energy dependence of the $(0,\ 0,\ \frac{9}{2})_C$ reflection at 20 K in the σ–σ channel, measured at fixed wavevector. The experimental dependence has been corrected for multiple scattering and absorption effects. The solid and dashed lines represent simulations with charge order (a) and without charge order (b). Although the dependence was measured in the σ–σ channel, the leakthrough from the σ–π channel was measured to be ∼0.92% and shows the σ–π simulation is shown with an attenuation of ∼99.08% relative to the σ–σ simulation. The simulation axes have been rescaled for the optimum fit, and the corrected intensity represents an order of magnitude estimate based on figure 4(a).

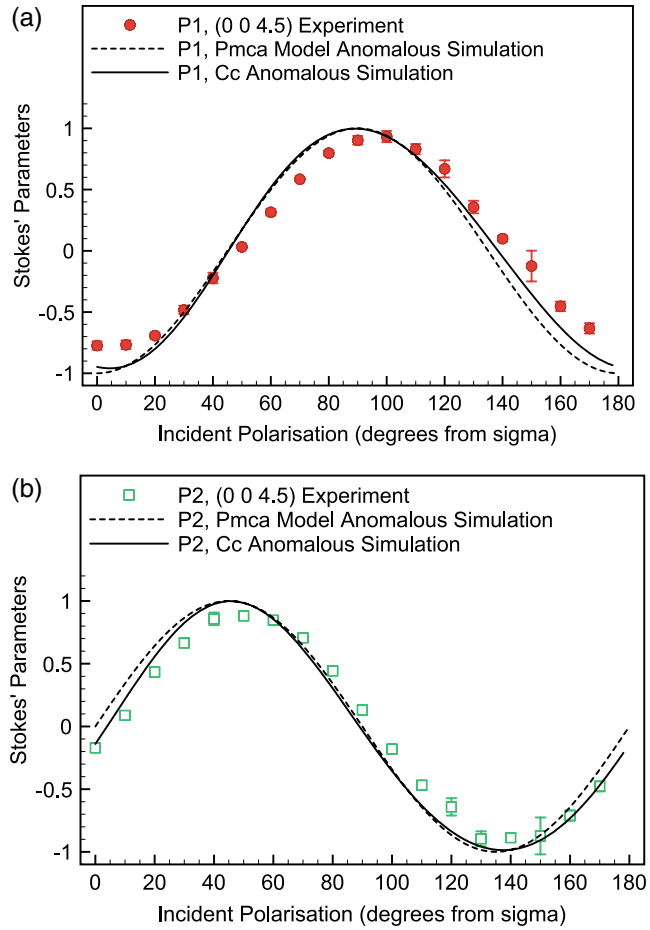

Figure 10. The polarization dependence of the $(0,\ 0,\ \frac{9}{2})_C$ reflection at 20 K. The energy is tuned to 7.120 keV, and the crystal orientated such that $\phi = 8.4°$. The dashed lines represent the simplified ATS scattering model in the *Pmca* unit cell, while the solid line represents ATS scattering produced using the full *Cc* structure, using FDMNES.

Before beginning a detailed analysis of the polarization results, we note from figures 10 and 11 that the $(0,\ 0,\ \frac{9}{2})_C$ and $(0\ 0\ 5)_C$ reflections have very different polarization dependences, and therefore completely different origins. The $(0,\ 0,\ \frac{9}{2})_C$ analysis shows that the scattered light has been significantly rotated, while the $(0\ 0\ 5)_C$ reflection displays the opposite, i.e. little change from incident to scattered polarization. It thus becomes immediately apparent that the $(0,\ 0,\ \frac{9}{2})_C$ reflection cannot be the result of charge order.

For the case of the $(0,\ 0,\ \frac{9}{2})_C$ reflection we present both a simplified model and an authentic model based on the charge ordered *Cc* structure using FDMNES. The *Pmca* model represents a highly simplified model, where the scattering factors from each inequivalent site are taken as equal, rather than being complex non-equal values. This is presented as a comparison to the complete treatment produced using FDMNES. The $(0,\ 0,\ \frac{9}{2})_C$ data, shown in figure 10, gives good agreement with the structural ATS scattering, with both models showing similar dependences. However, it is also interesting to examine the nonlinear, *pseudo* P_3, component of the scattered polarization, figure 12. Here, we see that a significant proportion of the scattered light has become nonlinearly polarized, and although the simulation has failed to fully predict the observed phenomena, it has replicated the general trend. For the simulation, this component is circularly polarized, which we are unable to measure directly. This component is too large to be from any nonlinear polarization effects at the phase plate, or from any interference from magnetic scattering at the iron K-edge, where the iron atoms have a magnetization of $\approx 4.2\ \mu_B$. The principle behind this effect is that subtly different scattering factors of each iron site introduce different complex coefficients into the structure factor. This can be seen through the simplified model (dashed line) which, by assuming each site (B1, B2, etc) has the same anisotropic scattering factor, fails to predict the circular component. We would thus expect to see this effect at other ATS reflections in alternative materials which also contained the same elements in different environments.

The result of the polarization analysis at the $(0\ 0\ 5)_C$ can be seen in figure 11, where it is apparent that the dominant factor is the isotropic Thomson charge scattering term f^0.

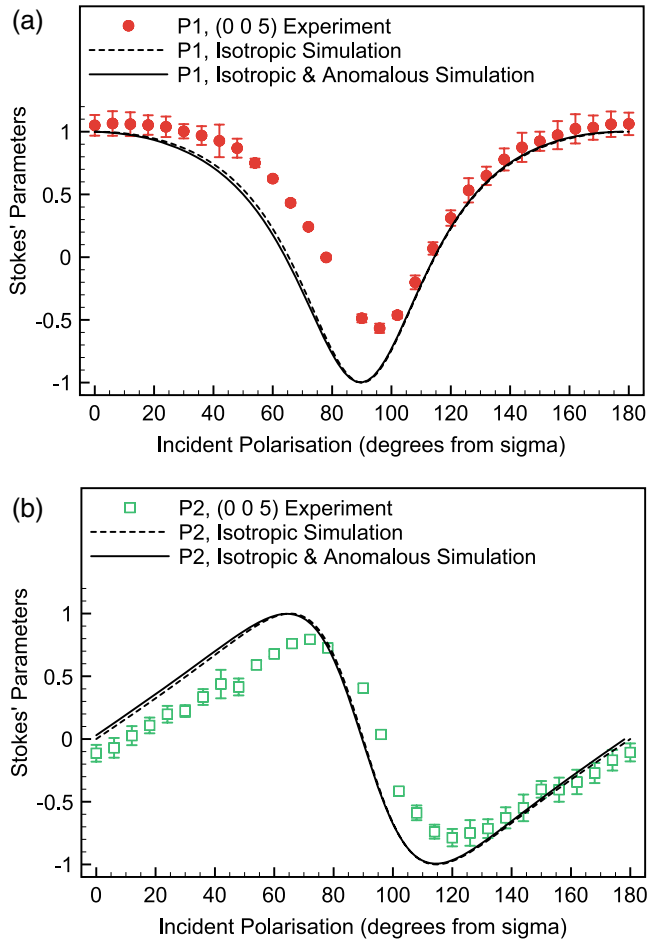

Figure 11. The polarization dependence of the $(0\ 0\ 5)_C$ reflection at 20 K. The energy is tuned to 7.120 keV and the crystal oriented such that $\phi = 8.4°$. The dashed line represents the isotropic Thomson scattering, while the solid line represents scattering produced using both Thomson and anomalous components. Both simulations were produced using the full Cc structure in FDMNES.

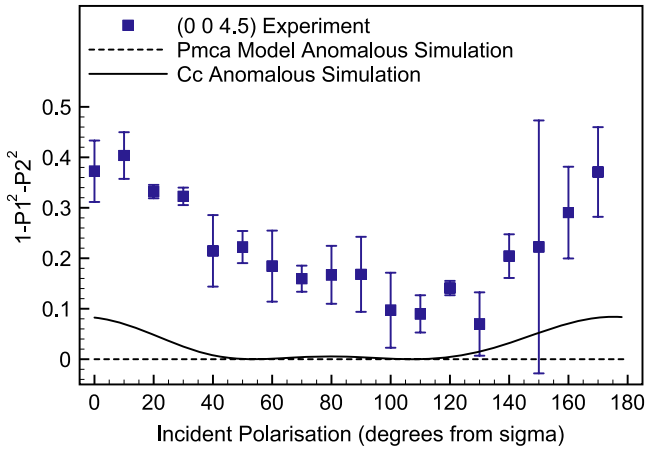

Figure 12. The square of the nonlinear component of the polarization dependence of the $(0,\ 0,\ \frac{9}{2})_C$ reflection at 20 K. The energy is tuned to 7.120 keV and the crystal oriented such that $\phi = 8.4°$. An upper limit for the measure of the nonlinear polarization component can be inferred by subtracting the intensities of the linear components of the polarization; P_1^2 and P_2^2. The dashed line represents the simplified ATS scattering model in the $Pmca$ unit cell which neglects the different scattering factors between each site, while the solid line represents ATS scattering produced using the full Cc structure, using FDMNES. The large error bars result as this analysis contains all nonlinear components, including unpolarized scatter.

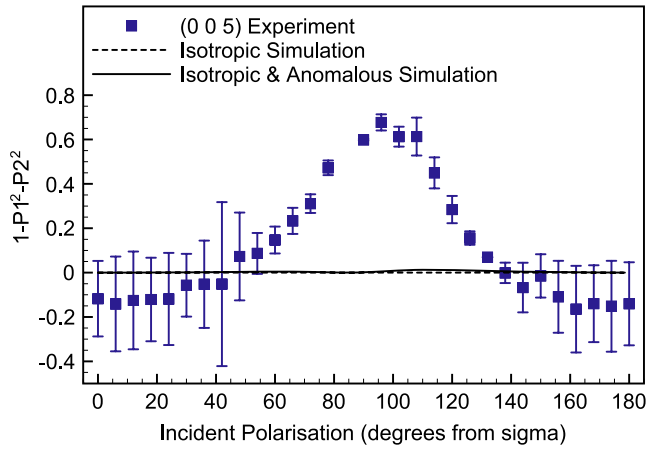

Figure 13. The square of the nonlinear component of the polarization dependence of the $(0,\ 0,\ 5)_C$ reflection at 20 K. The energy is tuned to 7.120 keV and the crystal orientated such that $\phi = 8.4°$. The dashed line represents the isotropic Thomson scattering, while the solid line represents scattering produced using both Thomson and anomalous components. Both simulations were produced using the full Cc structure in FDMNES. The large error bars result as this analysis contains all nonlinear components, including unpolarized scatter.

Indeed, the addition of the isotropic and anisotropic anomalous terms appears to have little effect on the simulation. However, it is clear that, although the simulation again follows the trend observed experimentally, the agreement is less compelling. In figure 11(a) there is clearly a large difference between the experimental and simulated data close to 90°. By again considering the nonlinear component we can see where the difference arises, figure 13.

This *pseudo* P_3 component is much larger than for the $(0\ 0\ \frac{9}{2})_C$ reflection. Although difficult to see in figure 13, the simulation does indeed predict a significant circular component, with approximately half of the scattered intensity from the anomalous contribution in the right and left circularly polarized channels. The predicted *pseudo* P_3 values of figure 13 are particularly small however, as the right and left circular components have very similar values. The circularly polarized components produced by the simulation are generated through the anomalous terms, as for the $(0\ 0\ \frac{9}{2})_C$ reflection. However, it is interesting to note that the addition of the Thomson isotropic terms to the simulation results in small changes to the simulation.

To summarize our main points: on the basis of our energy and polarization dependences we believe that the appearance of the $(0\ 0\ \frac{1}{2})_C$ type reflections can be explained as a result of the structural phase transition at T_V with no need to invoke any charge or orbital order models. This is the same conclusion reached in the recent soft x-ray study by Wilkins *et al* [31]; however, the soft x-ray study by Schlappa *et al* [30] uses the appearance of the reflection as evidence for

orbital ordering, which is not necessarily the case. However, as the appearance of ATS reflections as a first-order phase transition is a result of some local symmetry breaking, this may raise orbital degeneracy and so be linked to orbital order. Interference between the inequivalent iron sites results in a significant contribution becoming nonlinearly polarized. The $(0,\ 0,\ 2n+1)_C$ type resonant reflections are due to charge order (in agreement with hard [8] and soft [30] x-ray studies) and contain significant components from the isotropic and anomalous terms. The appearance of a large nonlinearly polarized component is again due to the interference of the anomalous terms at the inequivalent iron sites. However, the interference of the isotropic component *with* this is also important. We note here that, while the simulations produced do not fully replicate the experimental data in every aspect, they provide an acceptable approximation and indicate the physical processes involved in producing the experimental result. In this case it is an incomplete knowledge of the structure of magnetite that leads to the disagreement between the experimental and simulated data. Magnetite is a ferociously complex material, and here we have shown that simply by applying the previously reported electronic structure, reality can be approximated to a high degree.

5. Conclusion

In conclusion we have observed the $(0,\ 0,\ \frac{1}{2})_C$ and $(0\ 0\ 1)_C$ reflections at the iron K-edge and attributed their origins predominantly to ATS scattering and charge order, respectively. We have demonstrated this using both the energy spectra and the technique of full polarization analysis. We also report the conversion of linear to nonlinearly polarized light, and explain the origin through the complex structure of magnetite alone. However, we are unable to replicate the experimental data completely, demonstrating the difficulty in obtaining the low temperature electronic structure of magnetite by even the most discriminating techniques.

Acknowledgments

The authors wish to thank the ESRF and ID 20 for the beamtime and experimental support. SRB and PDH would like to thank EPSRC for funding. The work at Brookhaven National Laboratory is supported by the Office of Science, US Department of Energy, under contract no. DE-AC02-98CH10886. TAWB and PDH would like to thank STFC for financial support. SRB thanks R D Johnson for critical reading.

References

[1] Blackman M 1983 *Contemp. Phys.* **24** 319–31
[2] Verwey E J W and Heilmann E L 1947 *J. Chem. Phys.* **15** 4
[3] Anderson P W 1956 *Phys. Rev.* **102** 4
[4] Leonov I, Yaresko A N, Antonov V N and Anisimov V I 2006 *Phys. Rev.* B **74** 165117
[5] Nazarenko E, Lorenzo J E, Joly Y, Hodeau J L, Mannix D and Marin C 2006 *Phys. Rev. Lett.* **97** 056403
[6] Jeng H T, Guo G Y and Huang D J 2006 *Phys. Rev.* B **74** 195115
[7] Leonov I, Yaresko A N, Antonov V N, Korotin M A and Anisimov V I 2004 *Phys. Rev. Lett.* **93** 146404
[8] Lorenzo J E, Mazzoli C, Jaouen N, Detlefs C, Mannix D, Grenier S, Joly Y and Marin C 2008 *Phys. Rev. Lett.* **101** 226401
[9] Joly Y, Lorenzo J E, Nazarenko E, Hodeau J L, Mannix D and Marin C 2008 *Phys. Rev.* B **78** 134110
[10] Wright J P, Attfield J P and Radaelli P G 2001 *Phys. Rev. Lett.* **87** 266401
[11] Wright J P, Attfield J P and Radaelli P G 2002 *Phys. Rev.* B **66** 214422
[12] Jeng H T, Guo G Y and Huang D J 2004 *Phys. Rev. Lett.* **93** 156403
[13] Uzu H and Tanaka A 2008 *J. Phys. Soc. Japan* **77** 074711
[14] Kanazawa M, Hagaiwara K, Kokubun J and Ishida K 2002 *J. Phys. Soc. Japan* **71** 1765–70
[15] García J, Subías G, Proietti M G, Renevier H, Joly Y, Hodeau J L, Blasco J, Sánchez M C and Bérar J F 2000 *Phys. Rev. Lett.* **85** 578
[16] García J, Subías G, Proietti M G, Blasco J, Renevier H, Hodeau J L and Joly Y 2001 *Phys. Rev.* B **63** 054110
[17] Subías G, García J, Blasco J, Proietti M G, Renevier H and Sánchez M C 2004 *Phys. Rev. Lett.* **93** 156408
[18] Brabers V A M 1971 *J. Cryst. Growth* **8** 26
[19] Kim-Ngan N T H, Soszka W, Tarnawski Z and Kozlowski A 2004 *Physica* B **353** 164–8
[20] Shepherd J P, Koenitzer J W, Aragón R, Spalek J and Honig J M 1991 *Phys. Rev.* B **43** 8461
[21] Honig J M 1995 *J. Alloys Compounds* **229** 24–39
[22] Mazzoli C, Wilkins S B, DiMatteo S, Detlefs B, Detlefs C, Scagnoli V, Paolasini L and Ghigna P 2007 *Phys. Rev.* B **76** 195118
[23] Detlefs B, Wilkins S B, Caciuffo R, Paixão J A, Kaneko K, Honda F, Metoki N, Bernhoeft N, Rebizant J and Lander G H 2008 *Phys. Rev.* B **77** 024425
[24] Johnson R D, Bland S R, Mazzoli C, Beale T A W, Du C H, Detlefs C, Wilkins S B and Hatton P D 2008 *Phys. Rev.* B **78** 104407
[25] Calhoun B A 1954 *Phys. Rev.* **94** 1577
[26] Renninger M 1937 *Z. Phys.* **106** 141–76
[27] Hecht E 2002 *Optics* 4th edn (Reading, MA: Addison-Wesley)
[28] Templeton D H and Templeton L K 1994 *Phys. Rev.* B **49** 14850
[29] Dmitrienko V E 1983 *Acta Crystallogr.* A **39** 29–35
[30] Schlappa J, Schussler-Langeheine C, Chang C F, Ott H, Tanaka A, Hu Z, Haverkort M W, Schierle E, Weschke E, Kaindl G and Tjeng L H 2008 *Phys. Rev. Lett.* **100** 026406
[31] Wilkins S B, Matteo S D, Beale T A W, Joly Y, Hatton P D, Bencok P, Yakhou F, Mazzoli C and Brabers V A M 2009 *Phys. Rev.* B **79** 201102
[32] García J, Subías G, Herrero-Martín J, Blasco J, Cuartero V, Sánchez M C, Mazzoli C and Yakhou F 2009 *Phys. Rev. Lett.* **102** 176405
[33] Hagiwara K, Kanazawa M, Horieand K, Kokubun J and Ishida K 1999 *J. Phys. Soc. Japan* **68** 1592
[34] Uzu H and Tanaka A 2006 *J. Phys. Soc. Japan* **75** 043704
[35] Huang D J, Lin H J, Okamoto J, Chao K S, Jeng H T, Guo G Y, Hsu C H, Huang C M, Ling D C, Wu W B, Yang C S and Chen C T 2006 *Phys. Rev. Lett.* **96** 096401
[36] Joly Y 2001 *Phys. Rev.* B **63** 125120–9
[37] Hedin L and Lundqvist S 1971 *J. Phys. C: Solid State Phys.* **4** 2064